Long-term solar water and CO₂ splitting with photoelectrochemical BiOI-BiVO₄ tandems

Virgil Andrei,[1,2†] Robert A. Jagt,[3†] Motiar Rahaman,[1] Leonardo Lari,[4] Vlado K. Lazarov,[4] Judith L. MacManus-Driscoll,[3*] Robert L. Z. Hoye,[5*] and Erwin Reisner[1*]

[1] Yusuf Hamied Department of Chemistry, University of Cambridge, Lensfield Road, Cambridge CB2 1EW, United Kingdom.
[2] Optoelectronics Group, University of Cambridge, Cavendish Laboratory, J J Thomson Avenue, Cambridge CB3 0HE, United Kingdom.
[3] Department of Materials Science and Metallurgy, University of Cambridge, 27 Charles Babbage Rd, Cambridge CB3 0FS, United Kingdom.
[4] Department of Physics, University of York, Heslington, York YO10 5DD, United Kingdom.
[5] Department of Materials, Imperial College London, Exhibition Road, London SW7 2AZ, United Kingdom.
*Correspondence to: jld35@cam.ac.uk (J.L.M.-D.), r.hoye@imperial.ac.uk (R.L.Z.H.), reisner@ch.cam.ac.uk (E.R.).
† These authors contributed equally.

Photoelectrochemical (PEC) devices have been developed for direct solar fuel production, but the limited stability of submerged light absorbers hampers their commercial prospects.[1,2] Here, we demonstrate photocathodes with an operational H₂ evolution activity over weeks, by integrating a BiOI light absorber into a robust, oxide-based architecture with a graphite paste conductive encapsulant. In this case, the activity towards proton and CO₂ reduction is mainly limited by catalyst degradation. We also introduce multiple-pixel devices as an innovative design principle for PEC systems, displaying superior photocurrents, onset biases and stability over corresponding conventional single-pixel devices. Accordingly, PEC tandem devices comprised of multiple-pixel BiOI photocathodes and BiVO₄ photoanodes can sustain bias-free water splitting for 240 h, while devices with a Cu₉₂In₈ alloy catalyst demonstrate unassisted syngas production.

The stability of Earth-abundant light absorbers in aqueous media remains one of the key issues hindering solar fuel production on a large-scale[1,2]. While great efforts have been made to build combinatorial material libraries in pursuit of the "ideal" light absorber[3,4], these only reaffirmed the existing compromise between performance and stability. Besides low bandgap semiconductors (e.g. silicon), oxides have long been seen as a more robust, easy to fabricate alternative, but they also suffer from inherently low charge carrier mobilities and high non-radiative recombination rates[5]. Efforts have been made to address their limitations through chemical tuning by mixing together metal cations (*i.e.*, multicomponent metal oxides) or anions (*e.g.*, oxyhalides). Recently, the introduction of charge selective layers, a common practice in the photovoltaic (PV) community, offered a way to improve the photovoltage and photocurrent through effective charge extraction, while increasing stabilities up to ≈100 h[6,7]. In this case, dedicated electron (ETL) and hole transport layers (HTL) replaced the passivating coatings commonly employed in the PEC community, resulting in heterojunction photoelectrodes directing the photoexcited charges towards the catalyst (as opposed to classical photoelectrodes with semiconductor-electrolyte junctions).

Here, we emphasize the benefits of this emerging concept using the largely underexplored BiOI light absorber. Whilst the benign BiOI[8,9] is better known for photocatalytic pollutant/dye degradation[10], or simply as an intermediate in the BiVO₄ photoanode synthesis[11], there have been few studies on its PEC properties, due to its low photocurrent and rapid degradation in aqueous media[12,13]. In our case, we report a four-orders of magnitude increase in the overall stability of BiOI photocathodes for H₂ evolution, from minutes to weeks, by sandwiching the light absorber in a PV-inspired architecture[14]. We report similar stabilities when combining the BiOI

photocathode (Fig. 1a) with a BiVO₄ photoanode in a tandem configuration, providing a proof-of-principle for stable oxide-based PEC water splitting. On this occasion, we also reveal new insights into optimal device design and degradation pathways. To this end, we introduce a multiple-pixel design as a promising alternative to conventional single-pixel photoelectrodes, enabling an extension of the device scope to CO₂ splitting.

The BiOI PV devices have an inverted (*p-i-n*) oxide-based architecture, with a polycrystalline NiO$_x$ HTL, and polycrystalline ZnO ETL conformally covering the BiOI platelets (Fig. 1a,d, Supplementary Fig. 1)[14,15]. BiOI has a layered crystal structure (Supplementary Fig. 2), leading to anisotropic transport properties, in which lower effective masses (i.e. higher carrier mobilities) occur in the in-plane direction[16]. To improve charge extraction, the BiOI layers should have an [ab0] preferred orientation (i.e. upward-slanted BiOI platelets), such that the high-mobility planes connect the bottom and top charge transport layers. This has been obtained by controlling the process parameters during the growth of BiOI by chemical vapor deposition (CVD; see ref. 17 for discussion).

Eight individual 0.045 cm² pixels or a larger 0.25 cm² pixel were prepared onto 1.2×1.2 cm² ITO glass substrates, to form so-called "8-pixel" or "single-pixel" BiOI PV devices. On each 8-pixel device, 3-7 pixels are normally functional, whereas the rest are faulty. We prepared 8-pixel devices on 16 substrates (128 total pixels) and found that 81 pixels were functional. These 81 pixels displayed an average open circuit voltage (V_{OC}) of 0.69 ± 0.06 V, short circuit density (J_{SC}) of -4.3 ± 0.4 mA cm⁻² and power conversion efficiency (PCE) of 1.2 ± 0.2% (see box charts in Supplementary Fig. 3). In comparison, larger 0.25 cm² single-pixel samples resembling typical PEC devices only showed a V_{OC} of 0.53 ± 0.06 V and J_{SC} of -1.6 ± 0.3 mA cm⁻² (Fig. 1e, Supplementary Figs. 4, 5). The higher performance of the small pixels could be traced back to a reduction in shunting losses, as indicated by their increased V_{OC} and decreased dark currents (Supplementary Fig. 4). In contrast, a higher total number of pinholes and macroscopic defects is likely to be present on a larger-pixel device, as described in Supplementary Fig. 6.

The PV stability was investigated for 120 h in a N₂ environment at room temperature, at 0 V bias. After an initial faster decay, the short circuit current density remained stable for >100 h under continuous 1 sun illumination (Fig. 1g). A partial photocurrent recovery was observed when maintaining the device in the dark for 1 h every 24 h, manifesting through transient "spikes" in photocurrent lasting for up to 6 h (Fig. 1f), which resembled the behavior observed during long-term photocathode testing (see Fig. 2b below). This degradation and subsequent recovery when left in the dark has also been observed in metal halide perovskites and was caused by the formation of light-activated meta-stable deep-level trap
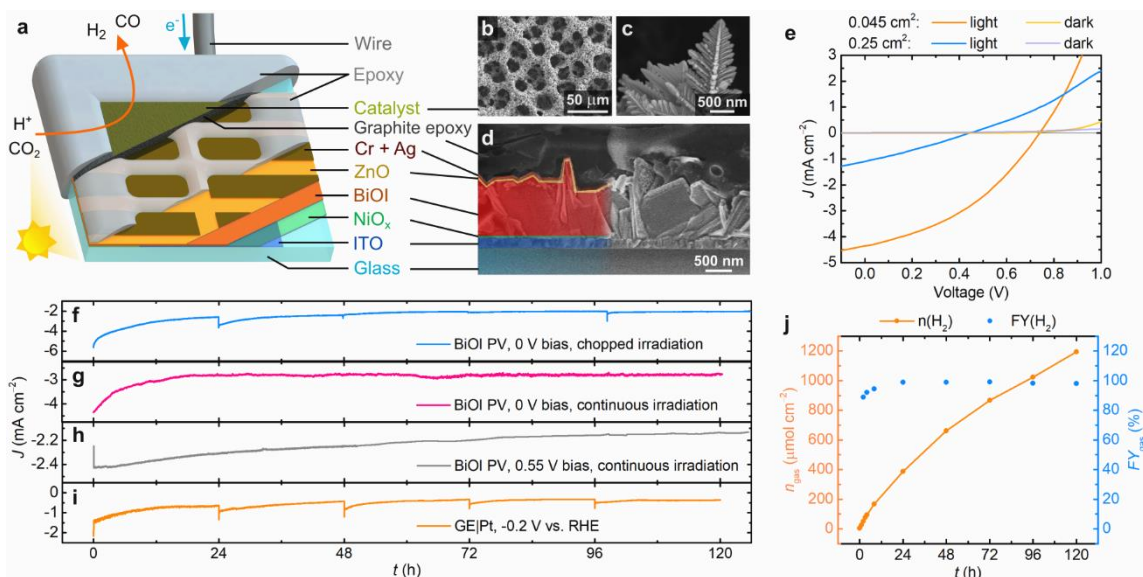
Fig. 1 | Performance of the individual photovoltaic and electrocatalytic components of the BiOI photocathodes. a, Schematic depiction of the BiOI photocathode with its components. **b,c**, Scanning electron microscopy (SEM) images of the dendritic $Cu_{92}In_8$ foam catalyst for CO_2 reduction. **d**, False color SEM image of the encapsulated device architecture. **e**, Examples of J-V curves for the underlying 0.045 and 0.25 cm^2 BiOI PV cells. **f-i**, Long-term stability tests. **f-h**, 0.045 cm^2 BiOI PV devices are operated at 0 V (**f,g**) and 0.55 V bias (**h**).The PV cells are characterized under chopped (**f**, 1 h dark - 24 h light cycles), or continuous (**g,h**) light irradiation. **i**, H_2 evolution with a dark GE|Pt electrode (-0.2 V vs. RHE, 0.1 M potassium borate (KB_i), 0.1 M K_2SO_4, pH 8.50, under N_2). **j**, Cumulative amounts of H_2 and faradaic yields (FY) for GE|Pt during the 120 h test shown in (**i**).

states[18]. A smaller photocurrent decay (retaining 88% of the initial current after 125 h) was observed when operating the devices at 0.55 V applied bias (Fig. 1h), which resembles the applied potential in a PEC tandem device (see Supplementary Fig. 22) and is closer to the PV maximum power point conditions. This encouraging intrinsic stability of the BiOI PV system was supported by J-V curves recorded before and after the 125 h test (Supplementary Fig. 7).

Integrated electrodes possessing photocathode functionality were next fabricated by interfacing BiOI photovoltaic cells with a Pt electrocatalyst. For this purpose, the working ITO|NiO$_x$|BiOI|ZnO|Cr|Ag pixels were encapsulated with conductive graphite epoxy (GE) paste, while a 5 nm Pt film was sputtered on top (see Methods). These buried PV photocathodes (noted BiOI|GE|Pt, see Fig. 1a,d and Supplementary Figs. 8, 9 for full structure) were characterized in a 3-electrode, 2-compartment system, under simulated solar irradiation (AM1.5G, 100 mW cm^{-2}, see Methods, Fig. 2). BiOI photocathodes were assembled from both 8-pixel and one-pixel PV devices with similar total photoactive areas, to compare the effect of the device architecture on the PEC performance (Fig. 2, Supplementary Figs. 10, 11). Each 8-pixel device formed the basis for a multiple-pixel photocathode, whereas the inactive area and damaged pixels were covered with epoxy (Supplementary Fig. 12). This pixel preselection could avoid pinholes and macroscopic defects in the layered device structure, thereby sustaining the high photocurrent and photovoltage of the individual small pixels on a larger total photoactive area.

A BiOI|GE|Pt photocathode with seven 0.045 cm^2 pixels amounting to a 0.315 cm^2 total photoactive area (*i.e.*, 0.315 (7×0.045) cm^2 device) achieved an initial photocurrent density beyond -4 mA cm^{-2} at 0 V against the reversible hydrogen electrode (RHE), a significant improvement over previously-reported n-type BiOI photoanodes that could only sustain photocurrents below 0.1 mA cm^{-2} for a few minutes[12,13]. In our case, a built-in potential is created when sandwiching the intrinsic BiOI between NiO$_x$ and ZnO, which directs electrons

towards the electrocatalyst (Supplementary Figs. 8, 9, 13). Hence, the multiple-pixel photocathode displayed an onset for H_2 evolution at 0.7 V vs. RHE, which is comparable with those of state-of-the-art Cu_2O[6] and silicon[19] heterojunction photocathodes. Cyclic voltammetry (CV) traces resembled the J-V curves in Fig. 1e, with a 0.315 (7×0.045) cm^2 device displaying a ≈0.2 V onset shift, a twofold increase in photocurrent density and 2.5 times increase in absolute photocurrent at 0 V vs. RHE over the 0.25 cm^2 single-pixel electrode of the same total substrate area (1.2×1.2 cm^2), which indicates the beneficial effect of the multiple-pixel arrangement (Fig. 2a, Supplementary Figs. 11e, 12).

Bare ITO|NiO$_x$|BiOI|ZnO devices without encapsulation degraded quickly at potentials below 0.1 V vs. RHE during CVs in an aqueous solution, yielding a metallic Bi phase (Supplementary Figs. 14-16). In contrast, long-term chronoamperometry of the encapsulated devices at 0 V vs. RHE revealed an encouraging stability of the oxide-based device architecture, with the 0.315 (7×0.045) cm^2 BiOI|GE|Pt photocathode operating for 500 h (Fig. 2b,c). The change in photocurrent density could be partly reverted by replenishing and re-purging the electrolyte solution every 24 h, with the transient photocurrent increase lasting for ≈12 h. A more gradual signal decay was attributed to nano-cracks forming over the GE|Pt catalyst interface[20] (Supplementary Fig. 17) and could be partly recovered after Pt redeposition.

To understand this degradation pattern, stability tests were also conducted for a series of electrocatalysts (Fig. 1i, Supplementary Figs. 18, 19). The H_2 evolution current of a GE|Pt electrode at -0.2 V vs. RHE displayed a similar variation over 24 h intervals to the photocurrents of the BiOI photocathodes (see examples in Fig. 1i and Supplementary Fig. 18a). A reversible 24 h variation was observed in case of the established robust FTO|RuO$_x$ electrocatalyst[21], which indicates this behavior is likely due to a pH build-up between the two compartments of the PEC cell. However, RuO$_x$ proved less suitable for our system, as low currents and high overpotentials were obtained when electrodepositing RuO$_x$ onto the non-oxidic GE (Supplementary
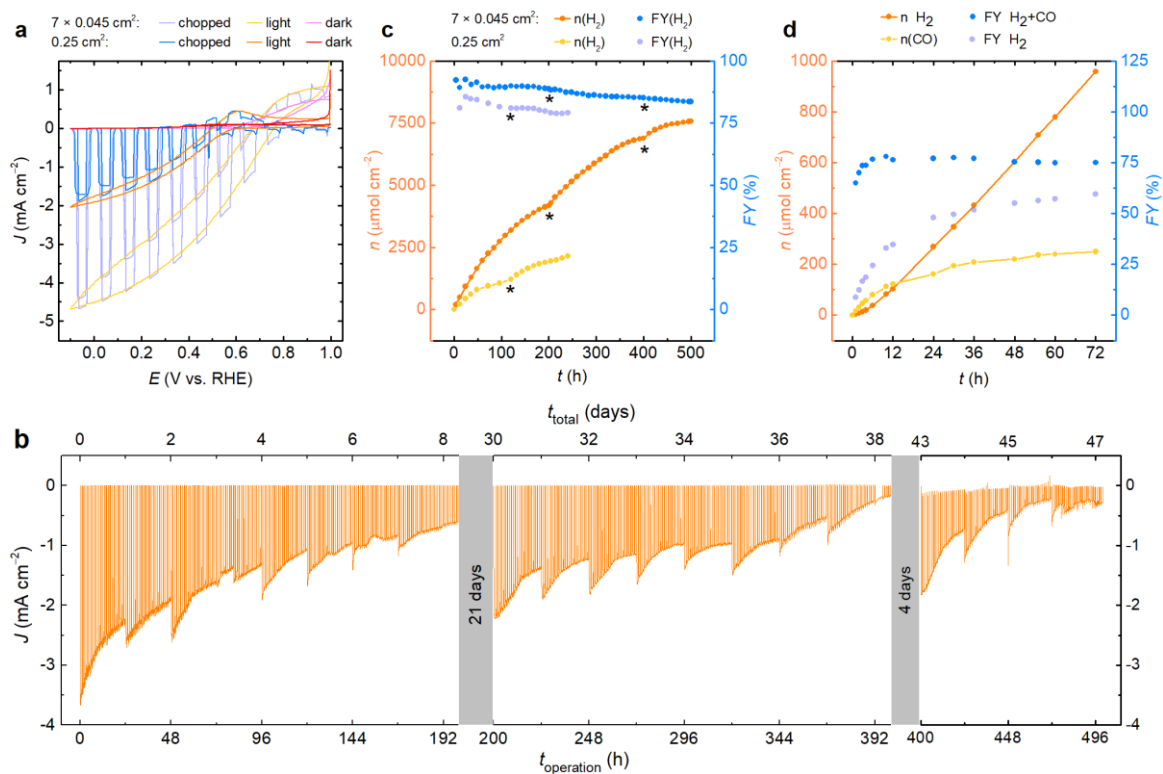
Fig. 2 | Photoelectrochemistry of the BiOI photocathodes. **a**, CV traces during chopped, continuous, and no light irradiation of BiOI|GE|Pt photocathodes consisting of one 0.25 cm² pixel (dark shades) and seven 0.045 cm² pixels (light shades). **b**, Long term chronoamperometric trace recorded at 0 V vs. RHE for the 0.315 (7×0.045) cm² photocathode. 5 nm Pt was redeposited by sputtering at the beginning of every longer testing interval (see grey areas). **c,d**, Cumulative amounts of products and faradaic yields obtained during stability tests for H_2 evolution (**c**, asterisks indicate Pt redeposition) and aqueous CO_2 reduction (**d**). Tests were conducted under simulated solar light irradiation (AM1.5G, 100 mW cm⁻²), at room temperature. A 0.1 M KB$_i$, 0.1 M K$_2$SO$_4$, pH 8.50 buffer solution was replaced and purged with N_2 every 24 h (**b,c**). A 0.5 M KHCO$_3$ solution, pH 7.4, was re-purged with CO_2 every 24 h for a 0.36 (8×0.045) cm² BiOI|GE|Cu$_{92}$In$_8$ photocathode (**d**).

Figs. 18, 19). Accordingly, the BiOI|GE|Pt photocathode current decay could be assigned to a combination of light absorber and catalyst (Fig. 1f-i) degradation. While a similar trend in the signal degradation/recovery was observed for both single and 7-pixel devices, the higher initial photocurrent of the 0.315 (7×0.045) cm² device resulted in a higher cumulative amount of product (Fig. 2c, Supplementary Fig. 11).

In case of the tandems, several configurations were investigated (Fig. 3 and Supplementary Figs. 20-22). A single-pixel 0.25 cm² BiOI - 0.25 cm² BiVO₄ device provided an initial photocurrent of ≈60 µA cm⁻² at no applied bias (Fig. 3a,b). The differences in V_{OC} and J_{SC} of the two device types were again reflected in the PEC performance, as tandems containing BiOI devices with 5-7 0.045 cm² working pixels presented an approx. 0.2 V earlier onset voltage for overall water splitting over their single-pixel counterparts (Fig. 3a, Supplementary Fig. 20a,c). The ≈ -0.4 V onset bias of multiple-pixel PEC tandem devices helped maintain the photocurrent density throughout the stability tests, in spite of PV or electrocatalyst degradation (Fig. 3b).

A 0.315 (7×0.045) cm² BiOI - 0.52 (8×0.065) cm² BiVO₄ tandem device (Supplementary Fig. 40) displayed a higher photocurrent density (up to ≈140 µA cm⁻², normalized for the BiOI area, corresponding to a 0.15% solar-to-H_2 efficiency) and higher product amounts over a 0.25 cm² BiOI - 0.25 cm² BiVO₄ tandem throughout 240 h tests at zero applied bias (Fig. 3b,c). A gradual decrease in the H_2 faradaic yield was observed over 120 h intervals, as O_2 accumulating inside the one-compartment reactor was reduced on the cathodic side (Fig. 3c).

These observations indicate that multiple small pixels are favorable to a single larger pixel of equivalent area, offering a new pathway for designing PEC devices. In a broad context, this encouraging stability of the BiOI devices places them among the

most stable PEC prototypes (which often decay within tens of hours)[1,22,23], moving closer to the values reported for state-of-the-art thin-film OPV[24], DSSC[25], or perovskite PV devices[26,27].

The BiOI devices were further interfaced to a porous CuIn alloy catalyst for photoelectrochemical syngas (CO + H_2 mixture) production from aqueous CO_2 [28]. The dendritic Cu$_{92}$In$_8$ alloy foam was synthesized by a template-assisted galvanostatic electrodeposition method (see Methods), with its composition developed towards long-term electrocatalytic CO production at a low overpotential of -0.3 V vs. RHE (see Figs. 1b,c, Supplementary Figs. 23-28 for characterization). The resulting BiOI|GE|Cu$_{92}$In$_8$ photocathodes showcased an initial CO:H_2 selectivity as high as 6.4:1 after 1 h at 0 V vs. RHE (Fig. 2d, Supplementary Fig. 30), while their early onset potential of 0.6 V vs. RHE provided sufficient overlap with the BiVO₄ photocurrent (Supplementary Fig. 29). Accordingly, BiOI|GE|Cu$_{92}$In$_8$ - BiVO₄ tandems demonstrated bias-free aqueous syngas production, displaying an onset voltage of -0.15 V, an initial CO:H_2 selectivity of 3.7:1 after 2 h and solar-to-H_2/CO efficiencies of 0.042% and 0.045%, respectively, after 12 h at 0 V applied bias (Fig. 3d, Supplementary Figs. 31, 32). BiOI photocathodes and PEC tandems sustained CO production for ≈24 h, following a similar trend observed during CO_2 electrolysis over Cu$_{92}$In$_8$ at -0.3 V vs. RHE (Supplementary Fig. 23). A faster decrease in the catalyst activity towards CO_2 reduction was likely due to the voltage and current fluctuations caused by light chopping. This manifested through an *in situ* phase transformation of the dendritic CuIn alloy, exposing a pure Cu phase which is mainly active towards H_2 evolution under the experimental conditions[28] (Supplementary Fig. 24). While photocatalytic CO_2 conversion using BiOI nanoparticles has been reported [29,30], these results provide the first demonstration of PEC CO_2 reduction using BiOI.
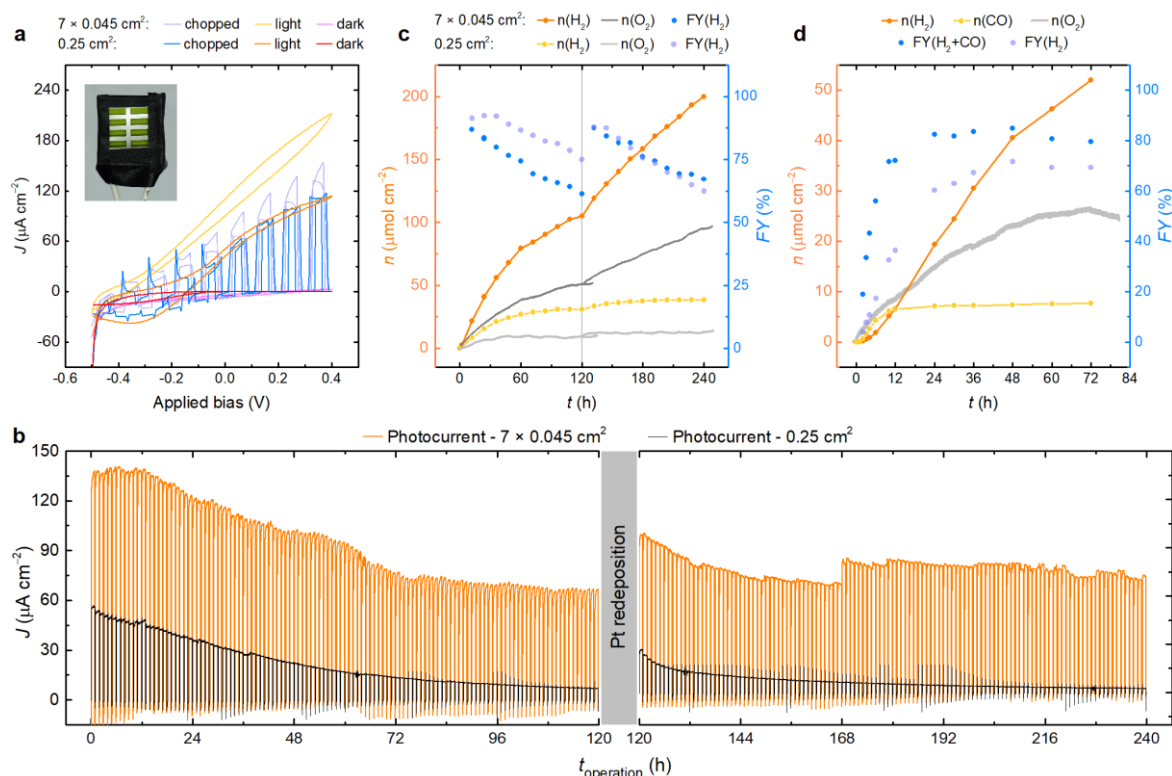
Fig. 3 | PEC performance of the BiOI-BiVO₄ tandem devices. a, CVs of a 0.315 (7×0.045) cm² BiOI - 0.52 (8×0.065) cm² BiVO₄ (photograph in inset) and a 0.25 cm² BiOI - 0.25 cm² BiVO₄ tandem under chopped, continuous, and no light irradiation. **b**, Photocurrent traces of bias-free tandems operated continuously over two 120 h intervals. One day was required in between to set up the experiment, redeposit the Pt catalyst, replace the buffer and purge it with N₂. **c,d**, Amounts of H_2, CO, O_2 and faradaic yields obtained during long-term stability tests at 0 V applied bias. Values are corrected for gas leakage (see Supplementary Discussion 1). Experiments were performed under simulated solar irradiation (AM 1.5G, 100 mW cm⁻²), at room temperature, in 0.1 M KB$_i$, 0.1 M K_2SO_4, pH 8.50, under N₂ for water splitting, and in a 0.5 M $KHCO_3$ solution, pH 7.4, under CO_2 for syngas production.

Moreover, BiOI-BiVO₄ is the first unassisted oxide tandem which can perform simultaneous syngas and oxygen evolution.

This work demonstrates that oxide-based semiconductors can approach and even challenge the performance of established light absorbers with an appropriate device architecture. A significant leap in the stability of an underexplored BiOI light absorber could be achieved by integrating it into a layered, buried-junction photocathode, which was encapsulated with state-of-the-art conductive graphite paste. Accordingly, BiOI photocathodes and unassisted BiOI-BiVO₄ tandem devices could operate for hundreds of hours. The BiOI devices provided a suitable photovoltage for H_2 production, as well as the more challenging CO_2 reduction to CO with an appropriate dendritic metal alloy foam catalyst. In this case, the photocurrent decay could be mainly traced back to electrocatalyst, but also device degradation. Multiple-pixel devices were also introduced as an enhanced design alternative to conventional PEC devices. These design principles offer new avenues to increase the performance and stability of other promising, yet moisture-sensitive semiconductors towards solar fuel production.

References

1. Kim, J. H., Hansora, D., Sharma, P., Jang, J.-W. & Lee, J. S. Toward practical solar hydrogen production – an artificial photosynthetic leaf-to-farm challenge. *Chem. Soc. Rev.* **48**, 1908–1971 (2019).
2. Sivula, K. & van de Krol, R. Semiconducting materials for photoelectrochemical energy conversion. *Nat. Rev. Mater.* **1**, 15010 (2016).
3. Yan, Q. *et al.* Solar fuels photoanode materials discovery by integrating high-throughput theory and experiment. *PNAS* **114**, 3040–3043 (2017).
4. Zhou, L. *et al.* Bi-containing n - FeWO₄ thin films provide the largest photovoltage and highest stability for a sub - 2 eV band gap photoanode. *ACS Energy Lett.* **3**, 2769–2774 (2018).
5. Rettie, A. J. E. *et al.* Combined Charge Carrier Transport and Photoelectrochemical Characterization of BiVO₄ Single Crystals: Intrinsic Behavior of a Complex Metal Oxide. *J. Am. Chem. Soc.* **135**, 11389–11396 (2013).
6. Pan, L. *et al.* Boosting the performance of Cu₂O photocathodes for unassisted solar water splitting devices. *Nat. Catal.* **1**, 412–420 (2018).
7. Andrei, V., Reuillard, B. & Reisner, E. Bias-free solar syngas production by integrating a molecular cobalt catalyst with perovskite–BiVO₄ tandems. *Nat. Mater.* **19**, 189–194 (2020).
8. Guo, Z. *et al.* Synthesis of BSA-coated BiOI @ Bi₂S₃ semiconductor heterojunction nanoparticles and their applications for radio / photodynamic / photothermal synergistic therapy of tumor. *Adv. Mater.* **29**, 1704136 (2017).
9. Mohan, R. Green bismuth. *Nat. Chem.* **2**, 336 (2010).
10. Cheng, H., Huang, B. & Dai, Y. Engineering BiOₓ (X = Cl , Br , I) nanostructures for highly efficient photocatalytic applications. *Nanoscale* **6**, 2009–2026 (2014).
11. Kim, T. W. & Choi, K.-S. Nanoporous BiVO₄ photoanodes with dual-layer oxygen evolution catalysts for solar water splitting. *Science* **343**, 990–994 (2014).
12. Hahn, N. T., Hoang, S., Self, J. L. & Mullins, C. B. Spray pyrolysis deposition and photoelectrochemical properties of n - type BiOI nanoplatelet thin films. *ACS Nano* **6**, 7712–7722 (2012).
13. Bhachu, D. S. *et al.* Bismuth oxyhalides: synthesis, structure and photoelectrochemical activity. *Chem. Sci.* **7**, 4832–4841 (2016).
14. Hoye, R. L. Z. *et al.* Strongly enhanced photovoltaic performance and defect physics of air-stable bismuth oxyiodide (BiOI). *Adv. Mater.* **29**, 1702176 (2017).
15. Huq, T. N. *et al.* Electronic structure and optoelectronic properties of bismuth oxyiodide robust against percent-level iodine-, oxygen-, and bismuth-related surface defects. *Adv. Funct. Mater.* **30**, 1909983 (2020).
16. Ganose, A. M., Cu, M., Butler, K. T., Walsh, A. & Scanlon, D. O. Interplay of orbital and relativistic effects in bismuth oxyhalides: BiOF, BiOCl, BiOBr, and BiOI. *Chem. Mater.* **28**, 1980–1984 (2016).
17. Jagt, R. A. *et al.* Controlling the preferred orientation of layered BiOI solar absorbers. *J. Mater. Chem. C* **102**, 10791 (2020).
18. Nie, W. *et al.* Light-activated photocurrent degradation and self-healing in perovskite solar cells. *Nat. Commun.* **7**, 11574 (2016).
19. Jang, J. *et al.* Enabling unassisted solar water splitting by iron oxide and silicon. *Nat. Commun.* **6**, 7447 (2015).
20. Pornrungroj, C. *et al.* Bifunctional perovskite-BiVO₄ tandem devices for uninterrupted solar and electrocatalytic water splitting cycles. *Adv. Funct. Mater.* **31**, 2008182 (2020).
21. Tilley, S. D., Schreier, M., Azevedo, J., Stefi, M. & Graetzel, M. Ruthenium oxide hydrogen evolution catalysis on composite cuprous oxide water-splitting photocathodes. *Adv. Funct. Mater.* **24**, 303–311 (2014).
22. Bae, D., Seger, B., Vesborg, P. C. K., Hansen, O. & Chorkendorf, I. Strategies for stable water splitting via protected photoelectrodes. *Chem. Soc. Rev.* **46**, 1933–1954 (2017).
23. Shen, X. *et al.* Defect-tolerant TiO₂ - coated and discretized photoanodes for >600 h of stable photoelectrochemical water oxidation. *ACS Energy Lett.* **6**, 193–200 (2021).
24. Burlingame, Q. *et al.* Intrinsically stable organic solar cells under high-intensity illumination. *Nature* **573**, 394–397 (2019).
25. Fakharuddin, A., Rajan, J., Brown, T. M., Fabregat-Santiago, F. & Bisquert, J. A

perspective on the production of dye-sensitized solar modules. *Energy Environ. Sci.* **7**, 3952–3981 (2014).

26. Saliba, M. *et al.* Incorporation of rubidium cations into perovskite solar cells improves photovoltaic performance. *Science* **354**, 206–209 (2016).

27. Bai, S. *et al.* Planar perovskite solar cells with long-term stability using ionic liquid additives. *Nature* **571**, 245–250 (2019).

28. Rahaman, M. *et al.* Selective CO production from aqueous CO_2 using a $Cu_{96}In_4$ catalyst and its integration into a bias free solar perovskite-$BiVO_4$ tandem device. *Energy Environ. Sci.* **13**, 3536–3543 (2020).

29. Wang, J. *et al.* Indirect Z - scheme BiOI/g-C_3N_4 photocatalysts with enhanced photoreduction CO_2 activity under visible light irradiation. *ACS Appl. Mater. Interfaces* **8**, 3765–3775 (2016).

30. Ye, L. *et al.* Synthesis of olive-green few-layered BiOI for efficient photoreduction of CO_2 into solar fuels under visible / near-infrared light. *Sol. Energy Mater. Sol. Cells* **144**, 732–739 (2016).

Methods

Materials. Indium tin oxide (ITO) coated glass (12 Ω □⁻¹, Colorado Concept Coatings LLC), BiI_3 (Sigma Aldrich, 99.99% metals basis), diethylzinc (Sigma Aldrich, 52 wt%), graphite (powder, <20mm, synthetic, Sigma-Aldrich), $KRuO_4$ (Sigma-Aldrich), H_3BO_3 (BioReagent, ≥99.5%, Sigma-Aldrich), K_2SO_4 (≥99%, ACS reagent, Sigma-Aldrich), $CuSO_4 \cdot 5H_2O$ (99.995%, Sigma-Aldrich), $In_2(SO_4)_3 \cdot xH_2O$, 99.99%, Sigma-Aldrich), H_2SO_4 (Suprapur 96%, Sigma-Aldrich), Cu foil (99.9%, Alfa Aesar), and $KHCO_3$ (≥99.5%, BioUltra, Sigma-Aldrich) were used without further purification.

BiOI PV devices. The ITO-coated glass substrates were cleaned using sonication for 15 min in 2-propanol and acetone, dried with compressed air and O_2 plasma treated (Zepto, Diener) for 10 min. Subsequently, NiO_x was deposited onto them by solution processing. 1 mol L^{-1} nickel nitrate hexahydrate (Sigma-Aldrich) solution in ethylene glycol (Sigma-Aldrich), complexed with 1 mol L^{-1} ethylenediamine, was prepared at room temperature and filtered through a 0.45 μm PTFE filter (Sigma-Aldrich). This solution was filtered again with a 0.45 μm PTFE filter, spread over the ITO-coated glass, and spin-coated at 5000 rpm for 45 s. The films were annealed at 100 °C for 30 min, followed by 300 °C for 1 h in air, then cooled by quenching on a piece of Al foil.

BiOI thin films were grown by chemical vapor deposition at atmospheric pressure, for details on the growth mechanisms also see ref. 17. A two-zone furnace with a quartz tube was used. The furnace was preheated to 360 °C in zones 1 and 2. Four substrates were attached to a microscope slide using silver paste (Electrolube) and loaded into the tube. 500 mg of BiI_3 was weighed into a crucible and placed close to the edge of the heating rod in zone 1 of the furnace. The substrates were at least 3 cm away from the center of the crucible. An $Ar:O_2$ gas mixture (19 mL min^{-1} Ar, 4.5 mL min^{-1} O_2) was introduced into the closed tube. Each growth run lasted for 50 min, which resulted in BiOI films that were ≈700 nm thick.

Finally, for the electron transport layer ZnO was deposited over the ITO/NiO_x/BiOI stack by atmospheric pressure chemical vapor deposition. For details also see ref. 31. In short, diethylzinc was used as the Zn precursor and O_2 gas (Air Products, <3 ppm H_2O) was the oxidant. 20 nm Cr and 100 nm Ag were sequentially thermally evaporated (0.1-0.2 nm s^{-1} rate; 2×10^{-6} mbar absolute base pressure) on top of the ZnO through a shadow mask. The device area is defined by the overlap between the Cr/Ag top electrode and the patterned ITO bottom electrode, and this was 4.5 mm^2 for each pixel.

PEC devices. The BiOI devices were encapsulated in three steps. The exposed wiring, damaged pixels and inactive area of the BiOI devices were first coated with Araldite 5-Minute Rapid epoxy (Supplementary Figs. 12, 40b). The active pixel areas were next coated with a conductive graphite epoxy (GE) paste, prepared by mixing 0.20 g Araldite Standard epoxy to 0.15 g graphite powder[32]. CO_2 reduction catalysts could also be attached to this fresh paste. Araldite 5-Minute Rapid epoxy was finally used to cover any remaining exposed edges and delimit the electrochemically active area (Supplementary Fig. 40a-f). A 5 nm thick Pt film was subsequently sputtered onto the exposed graphite epoxy as the hydrogen evolution catalyst (HEC). A RuO_x HEC was deposited onto FTO and GE electrodes by applying a current density of −30 μA cm^{-2} for 15 min, in an aqueous 1.3 mM $KRuO_4$ solution[21]. $BiVO_4$ photoanodes were deposited on FTO glass and subsequently coated with a $TiCoO_x$ (TiCo) water oxidation catalyst following reported procedures[33].

Photovoltaic characterization. Solar simulations were performed using an ABET Technologies Sun 2000 Solar Simulator and Keithley 2623A source-measure unit. The light source was a 450 W xenon lamp (Oriel) equipped with a Schott-K113 Tempax sunlight filter (Präzisions Glas & OptikGmbH) to match the emission spectrum of the lamp to the AM1.5G standard. The devices were all illuminated from the substrate (glass|ITO|NiO_x) side. Before measuring the devices, the solar simulator was calibrated with a silicon reference diode equipped with an infrared cut-off filter (KG-3, Schott). The scan rate was 100 mV s^{-1}. J-V curves of individual pixels were measured using 8-pin sample holders. A similar design can be adapted for large scale manufacturing, as detailed in Supplementary Fig. 33. Device values are reported for non-shunted pixels from different substrates.

Photoelectrochemical characterization. Photoelectrochemistry was conducted using Ivium CompactStat potentiostats and Newport Oriel 67005 solar light simulators with AM 1.5G optical filters, calibrated to 1 sun (100 mW cm^{-2}) using a certified Newport 1916-R optical power meter. PEC experiments were performed in a 0.1 M H_3BO_3, 0.1 M K_2SO_4 buffer solution (adjusted to pH 8.50 with 10 M KOH), without stirring, at room temperature, under N_2 atmosphere. The photocathodes were tested in a 3-electrode configuration with a Ag/AgCl/NaCl(sat) (Basi MW-2030) reference and a platinum mesh counter electrode. The potentials recorded against Ag/AgCl were converted to the RHE

scale using the equation E (V vs. RHE) = E (V vs. Ag/AgCl) + 0.059 V × pH + 0.197 V (at 298 K). The anodic and cathodic compartments were separated by a Selemion (AGC Engineering) ion exchange membrane. The 2-electrode tandem devices were characterized in a one compartment PEC cell (Supplementary Fig. 40i,j). The individual photocathodes were characterized without masking, whereas black tape surrounded the $BiVO_4$ photoactive area for the tandems. A mask was additionally employed in case of the 8-pixel devices, to define the irradiated area of the front $BiVO_4$ photoanode (Supplementary Fig. 40g,h). CO and H_2 quantification was conducted with a Shimadzu GC-2010 Plus gas chromatograph (GC). O_2 evolution was recorded using an Ocean Optics Fospor-R fluorescence oxygen sensor probe. Henry's law was used to account for the amount of dissolved gases[33]. The amounts of products evolved during continuous, long-term PEC tandem experiments were corrected using the leakage of the internal methane standard from the PEC reactor. For this purpose, an iterative model for the gas leakage was developed, based on the assumption that gases leak out at a rate proportional to their partial pressure at a given time (see Supplementary Discussion 1 for a mathematical description).

Additional PEC observations. Despite the good photocurrent overlap between BiOI and $BiVO_4$ (accountable for the early water splitting onset voltage, Supplementary Fig. 22), the devices only showed photocurrents below 200 μA cm^{-2}. This indicates that $BiVO_4$ acts as an effective light filter at wavelengths shorter than 500 nm, limiting the amount of light reaching the BiOI, which only absorbs below 650 nm (Supplementary Figs. 34, 35). Indeed, a similar photocurrent decrease was observed for the BiOI photocathodes when employing a 515 nm light filter (Supplementary Fig. 36).

A decrease in the dark current and increase in the onset bias of the BiOI|GE|Pt - $BiVO_4$ tandem devices was further observed under operation (Supplementary Fig. 37). This improvement may be due to the filling of trap states, where the continued exposure to light creates meta-stable trap states reducing the non-radiative recombination and dark current[18] (Supplementary Fig. 38). This hypothesis is supported by the increased open circuit voltage over time under continuous illumination (Supplementary Fig. 39). This lower dark current and higher photovoltage of the PV devices translate to a lower dark current and higher onset potential of the corresponding BiOI photocathodes and tandem devices.

Synthesis of the CO_2 reduction catalyst. The dendritic $Cu_{92}In_8$ alloy foam catalyst was synthesized by a dynamic hydrogen bubble template (DHBT) assisted electrodeposition method following a previously reported protocol (see ref. 28). An electropolished Cu foil was used as a substrate. The electrodeposition was carried out in a glass beaker containing copper sulfate and indium sulfate (0.025 M total) precursor salts in a 1.5 M H_2SO_4 electrolyte (pH ~ 0.5). A leak-free Ag/AgCl (satd. NaCl, BASi) electrode was used as reference, a Cu foil (4 × 4 cm^2) as counter, and the electropolished Cu foil substrate was used as working electrode in a three-electrode setup. A galvanostatic electrodeposition was performed by applying -3 A cm^{-2} current density for 60 s. After preparation, the catalyst was rinsed with Milli-Q water and dried under N_2 stream.

Electrochemical characterization. The $Cu_{92}In_8$ catalyst was electrochemically characterized in a two compartment H-cell separated by an anion exchange membrane (Selemion, AGC Engineering) using an Ag/AgCl (satd. NaCl, BASi) electrode as reference and a Pt mesh (99.9%, Alfa Aesar) as counter. The long-term CO_2 electrolysis was carried out at -0.3 V vs. RHE for five days in an aqueous 0.5 M $KHCO_3$ medium. Both cathode and anode chambers were purged with CO_2 every 24 h. The headspace was manually injected to a gas chromatograph (GC-2010 Plus, Shimadzu) to quantify the products.

Materials characterization. A TESCAN MIRA3 FEG instrument was used for SEM images of the CuIn alloy. The SEM was equipped with an Oxford Instruments Aztec Energy X-maxN 80 EDX system. Electron microscopy images of BiOI devices were taken on a FEI Nova NanoSEM. For the cross-sectional images, immersion mode is used to obtain high resolution images. High-resolution TEM imaging was performed using an aberration corrected JEOL 2200FS TEM operating at 200 kV. Images were acquired on a Gatan Ultrascan 1000US camera with 14 micrometer pixel size. Sample preparation was done by mechanical polishing followed by Ar^+ ion thinning using a Gatan PIPS precision ion polishing system as detailed in ref. 34. X-ray diffraction was performed on a Bruker D8 theta/theta system, using Cu Kα radiation (λ = 1.5406 Å). The total transmittance and reflectance spectra were acquired using an ultraviolet-visible-near infrared spectrophotometer (Shimadzu UV-3600) equipped with an integrating sphere.

Statistics. The reported average values are based on sample triplicates, with the errors corresponding to the standard deviation[35].

Data availability

References

31. Raninga, R. D. *et al.* Strong performance enhancement in lead-halide perovskite solar cells through rapid , atmospheric deposition of n-type buffer layer oxides. *Nano Energy* **75**, 104946 (2020).
32. Andrei, V., Bethke, K. & Rademann, K. Adjusting the thermoelectric properties of copper(I) oxide–graphite–polymer pastes and the applications of such flexible composites. *Phys. Chem. Chem. Phys.* **18**, 10700–10707 (2016).
33. Andrei, V. *et al.* Scalable triple cation mixed halide perovskite–$BiVO_4$ tandems for bias-free water splitting. *Adv. Energy Mater.* **8**, 1801403 (2018).
34. Lari, L., Lea, S., Feeser, C., Wessels, B. W. & Lazarov, V. K. Ferromagnetic InMnSb multi-phase films study by aberration-corrected (scanning) transmission electron microscopy. *J. Appl. Phys.* **111**, 07C311 (2012).
35. Harris, D. C. *Quantitative chemical analysis*. (W.H. Freeman and Co., 2007).

Acknowledgements

Author contributions

V.A., R.A.J., R.L.Z.H. and E.R. designed the project. R.A.J. and R.L.Z.H. developed and characterized the BiOI solar cells. V.A. developed the encapsulation, prepared the photoelectrodes and performed the photoelectrochemical characterization. M.R. designed, synthesized, and characterized the CO_2 reduction catalyst. L.L. and V.K.L. performed TEM characterization and data analysis. V.A. and R.A.J. drafted the manuscript. All authors contributed to the discussion and completion of the manuscript. J.L.M.-D. proposed the use of BiOI for optoelectronic applications, R.L.Z.H. and E.R. supervised the work.

Competing interests

The authors declare no competing interests.